Journal Homepage: http://ijcpe.uobaghdad.edu.iq
Iraqi Journal of Chemical and Petroleum Engineering
Vol. 25 No. 4 (December 2024) 123 – 137
EISSN: 2618-0707, PISSN: 1997-4884

Mathematical and experimental study of the direct contact membrane distillation method for desalination using a hydrophobic electrospun nanofibers membrane

Nawras N. Safi [a, *], Basma I. Waisi [b]

a Ministry of Construction and Housing and Municipalities Public, Iraq
b Department of Chemical Engineering, College of Engineering, University of Baghdad, Baghdad, Iraq

Abstract

This paper examines the performance of a Direct Contact Membrane Distillation (DCMD) system experimentally and theoretically. The system uses a super hydrophobic electrospun nanofiber membrane to desalinate water. Investigations were carried out into how the feed concentration, feed flow rate, and feed temperature affected permeate flux. as system operating parameters to aid in comprehending the factors impacting the DCMD process. The application of DOE and Taguchi methods achieved statistical optimization of the DCMD process's performance. In addition, the study of mass and heat transport in DCMD was described by a theoretical model. While the feed concentration (0- 210 g/L) significantly affected flux, the feed's temperature (35-55 °C) and flow rate (0.2-0.6 L/min) mostly dominated the impact on system performance. The created model numerically solved the DCMD process using MATLAB software, describing it as a system of nonlinear equations. Various operating conditions were used to investigate the efficiency of the superhydrophobic electrospun nanofiber membrane in treating 210 g/L NaCl salt water. Changing the feed temperature and concentration affected the hypothetically suggested path across the membrane, according to the simulation results presented in this paper. Excellent agreement was observed between the experiment results and the constructed model's predicted results. Every instance maintained a high salt rejection rate (over 99.9%). The DCMD produced a gain output ratio (GOR) of 0.87 and a temperature polarization coefficient of 0.78 to 0.91. The system achieved a maximum thermal efficiency of 73.5%. The optimal parameters, which are 70 g/L, 0.6 L/min, and 55°C.

Keywords: Modelling and Simulation; Super Hydrophobic Nanofiber Membrane; Membrane Distillation.

Received on 23/03/2024, Received in Revised Form on 10/06/2024, Accepted on 10/06/2024, Published on 30/12/2024

https://doi.org/10.31699/IJCPE.2024.4.12

1- Introduction

As a result of rising populations, expanding economies, and dwindling natural water supplies, many countries are facing significant water shortages [1]. The majority of the water on Earth is saltwater (97.5% of the total), but just a little fraction, 2.5% to be exact, is fresh and drinkable, making it ideal for use in various applications such as home and industrial water systems, as well as meeting agricultural needs. According to the most recent data from the "World Water Development Report," over 50% of the world's nations will be facing a shortage of water by 2030, and almost 75% of the world's population will likely face water shortages by 2050 [2, 3]. The development of potable water exporters has been a significant global issue. One of the most promising ways to create fresh water is by desalinating seawater and brackish water, which has been a worldwide problem for years due to the shortage of drinking water[4]. Among the most important commercial processes for supplying fresh water to various industrial and community sectors, seawater desalination has played an essential role in the socioeconomic development of many developing nations, particularly in North Africa and a small number of Middle Eastern nations[5]. Reverse osmosis (RO) is most often used to desalinate saltwater. The RO type accounts for over 60% of all desalination plants currently operating [6, 7]. Using various energy sources, desalination separates salty water into two components: combined with brine concentrate, which contains a significantly higher concentration of dissolved salts than the initial input water, and freshwater, which includes a lower concentration of dissolved salts [8]. With new, highly porous membranes created during the past 20 years, membrane distillation, or MD, has attracted much attention. Such membranes' performance is mainly dictated by their properties as well as the important process's operating parameters, such as temperature, concentration, and feed flow rate [9]. Electricity generated by nuclear power has increased dramatically over the past three decades, rising from 14% of total electricity generation in 2009 to nearly 19% in 2016. Recent articles claim that the world's nuclear power capacity will rise from 2009 levels by 2030. The primary method for generating nuclear energy is nuclear fission.

*Corresponding Author: Email: nawras.safi1507d@coeng.uobaghdad.edu.iq

Turbine generators, which produce electricity, rely on the heat produced by this process to create steam. Since it doesn't require burning fossil fuels, it's also thought to not release any greenhouse gases. The correct disposal of radioactive waste and other operational safety concerns, however, limit the applicability of this technique. A new word, "nuclear desalination," emerged from the use of nuclear power in desalination operations.[10] One definition of membrane distillation (MD) is that mass and heat are transmitted across a hydrophobic microporous membrane in a thermal process [11].

The fundamental benefit of membrane technology over conventional distillation processes is the membrane's ability to operate at low feeding temperatures. In contrast to more traditional membrane processes, such as RO, MD operates at a relatively low pressure [12, 13]. The four main kinds of MD configurations are defined by the way the vapour is removed via the side of the membrane that is hot [14]: direct contact membrane distillation (DCMD) which directly condenses vapor on the permeate side and inside the membrane module using cold water [15], vacuum membrane distillation (VMD) which the permeate side has a vacuum pump that pulls the volatile molecules out of the feed solution that lets the water vapor collect in the membrane unit or a separate condenser [16], air gap membrane distillation (AGMD) in which the vapor condenses inside the membrane module using a stagnant air layer situated at the permeate side halfway between the condensation surface and the membrane layer [17] and sweeping gas membrane distillation (SGMD) where condensation occurs in the outer member unit by utilizing a cold, inefficient gas that pulls vapor molecules from the cold side [18].

The following drawbacks of MD make it impractical for usage in commercial settings and so limit its potential as a separation method in industry: 1) reduced permeate flux compared to pressure-based membrane processes (2) the technical constraints of pore wetting and trapped air within membrane pores, which further limits the MD permeate flux due to increased mass transfer barrier [19, 20].

Several research projects that have the DCMD method discovered in the existing literature; between them, operating condition assessment using the response surface approach in the DCMD technique for desalination of seawater with PVDF-HFP membrane [9], A numerical utilizes computational fluid dynamics (CFD) models in three dimensions to study how corrugations impact DCMD modules [21], A Study on Experimental and Simulation Methods for the Desalination of Highly Saline Water by the Use of Direct Contact Membrane Distillation (DCMD) by commercial membrane [22], investigate the mass flux's sensitivity to the various parameters linked to direct contact membrane distillation (DCMD) to produce water through parametric sensitivity analysis [23]. The computational fluid dynamics (CFD) method was used to mathematically model the behavior used in the DCMD procedure under different operating circumstances [24]. Direct Contact Membrane Distillation: An Examination of the Plate and Frame Membrane Module as an Experimental Desalination performance of 3 wt.% NaCl solution by three-factor, three-level orthogonal experiment was designed [25], analyze the polarizations of temperature and concentration to improve the performance of direct contact membrane distillation utilizing the Navier-Stokes and species transportation equations, the flow, heat, and mass transfer properties of the flat sheet DCMD process are demonstrated [26]. In this study, we used MATLAB to create a DCMD heat and mass transfer model that accounts for the additional resistance to mass transfer that might not be immediately apparent through MD operations. The hypothetical path across the membrane represents this resistance, the thickness of the membrane, and the tortuosity, which are variables dependent on the operating conditions (temperature and concentration) to maximize the membrane's performance. This study used Matlab and a desirability approach to evaluate the main effects of the feed temperature, flow rate, and concentration of feed and to produce a gain output ratio (GOR) temperature polarization coefficient and achieve maximum thermal efficiency.

2- Theoretical model

Mass and heat transmission are two of the many complicated transport mechanisms that take place together in MD. In this work, several nonlinear equations resulting from the heat and mass balances were solved numerically to create a DCMD system model. This model utilized into account several assumptions, including that the system operates in a steady-state condition, that is only one direction of flow, the flow rate is laminar (the x direction), and that neglecting the heat lost from the system to the environment, the overall pressure is taken to remain constant at 1 atm along the water passing on the path. Considering that there is no wetting within the membrane layer, the feed solution's nonvolatile components, such as salt, are entirely removed.

Water vapor is diffused via a membrane with a uniform pore size (ignoring the distribution of pore sizes) and transports along a tortuous path. Water vapor can diffuse through the membrane because the air trapped within its holes remains stationary. The DCMD's transport mechanism method is illustrated schematically in Fig. 1 [27-29].

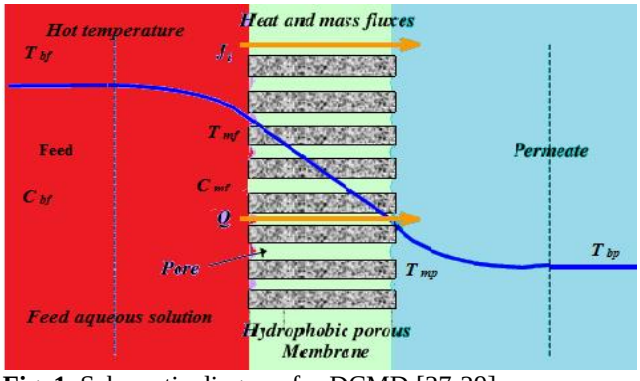

Fig. 1. Schematic diagram for DCMD [27-29]

2.1. Mass transfer

The three-step mass transfer process in MD begins with the vaporization of the hot feed at the liquid/gas interface, continues with the vapor's diffusion from the hot interface to the permeate interface via the pores of the membrane, and finally, with its condensation into the permeate side stream, driven by the vapor pressure difference [27, 30, 31].

The water vapor pressure differential between the feed and permeate sides is the primary generator of the mass flux through the membrane. This allows us to determine the permeate mass flux as [32-34]:

$$Jw = De * \Delta P_m = De * (P^\circ_{m,f} - P^\circ_{m,p}) \quad (1)$$

In which Jw and the equivalent diffusion coefficient represent the mass flux of permeate is denoted by *De*. The difference in vapor pressure at surfaces that cross a membrane is denoted as ΔP_m. The vapor pressures of the feed side at the surface of the membrane are $P^o_{m,f}$, and the vapor pressure of the permeate side is $P^o_{m,p}$.

Only the sodium chloride salinity affects the vapor pressure at the feed side, which must be included when the pressure is calculated [35].

$$P^\circ_{m,f} = p^o_{m,f} * a_{w,f} * X_{w,f} \quad (2)$$

$p^\circ_{m,f}$ is the pressure of water vapor at the surface of the membrane, as determined by the Antoine equation at temperatures (T_{mf}) [35].

$$p^\circ_{m,f} = exp\left[(23.1964) - \frac{3816.44}{T_{mf} - 46.13}\right] \quad (3)$$

$$X_{w,f} = (1 - X_{NaCl}) \quad (4)$$

$X_{w,f}$ is the water mole fraction in the feed. X_{NaCl} is the NaCl mole fraction in the feed. $a_{w,f}$ is the NaCl solution's water activity coefficient, which can be calculated as follows [35]:

$$a_{w,f} = 1 - 0.5\,(X_{NaCl}) - 10\,(X_{NaCl})^2 \quad (5)$$

$p^\circ_{m,p}$ is the pressure of water vapor at the surface of the membrane, as determined by the Antoine equation at temperatures (T_{mp}) [22, 36].

$$P^\circ_{m,p} = p^\circ_{m,p} = exp\left[(23.1964) - \frac{3816.44}{T_{mp} - 46.13}\right] \quad (6)$$

Gases and vapors can be transferred through porous media using three mechanisms. Three such models are the Knudsen, molecular diffusion, and Poiseuille flow models**.** In DCMD, the models of molecular diffusion and Knudsen flow are applicable. No hydrostatic pressure across the membrane is required because the pressure inside the membrane module is constant for both the feed and permeate solutions (about 1.0 atm). There is essentially no Poiseuille flow here [22, 36].

By dividing the Knudsen diffusion by the molecular diffusion, we determined the combined effect of the two diffusions. This ratio defines the mass transfer control mechanism α. The range of possible values for D_k α is from 0 to 1 [33].

$$De = \left[\frac{\alpha}{D_K} + \frac{1-\alpha}{D_M}\right]^{-1} \quad (7)$$

De refers to effective diffusion, D_K for Knudsen, and D_M for molecular diffusion. The expressions for D_K and D_M are as follows [1, 37]:

$$D_k = \left[\left(\frac{3 * \delta * \tau}{2 * \varepsilon * d_{pore}}\right) * \left(\frac{\pi * R * T_m}{8 * M_{olw}}\right)^{0.5}\right]^{-1} \quad (8)$$

$$D_M = \left(\frac{R * T_m * \delta * \tau * P\, d_{pore}}{M_{olw} * \varepsilon * PDwa}\right)^{-1} \quad (9)$$

Where δ represents the thickness of the membrane, ε refers to its porosity, R denotes the universal gas constant, d_{pore} shows the diameter of the pore, M_{olw} is the molecular weight of water molecules, and P is the total pressure inside the pore. For a water-air mixture usable between 273 and 373 K, the following expression can be used to determine the PD_{WA} value (Pa m^2/s), and Tm denotes the average temperature over the membrane's surfaces [20, 38, 39]:

$$PD_{WA} = 1.895 * 10^{-5} Tm^{2.072} \quad (10)$$

$$Tm = \frac{T_{mf} + T_{mp}}{2} \quad (11)$$

τ is like in the Mackie-Meares equation. The membrane porosity (ε) is frequently associated with the membrane tortuosity (also frequently constant) [20, 22, 40].

$$\tau = \frac{(2-\varepsilon)2}{\varepsilon} \quad (12)$$

2.2. Heat transfer

2.2.1. The movement of heat from the input side to the output surface of the membrane

The cooling law of Newton controls the convectional heat transfer that takes place in the feed boundary layer [20, 33, 40-42].

$$Q_f = h_f * (T_{bf} - T_{mf}) \quad (13)$$

Q_f is the convective heat flux (W/m^2), T_{bf} is the input and output hot feed stream's bulk temperature, hf is the boundary layer heat transfer coefficient at the membrane feed side, and T_{mf} is the average membrane feed side temperature.

Nusselt, Reynolds, and Prandtl dimensionless numbers used empirical correlations to get the heat transfer coefficient h_f [41, 43, 44].

$$h_f = \frac{Nu\, k}{D_h} \quad (14)$$

Where k is the fluid's average thermal conductivity at the feed side of the membrane, and Nu is the Nusselt number, which in the case of laminar flow is given by the following expression [44, 45]:

$$Nu = 1.86\,(Re\,Pr\,\frac{D_h}{l})^{0.33} \quad (15)$$

Where D_h is the hydraulic diameter of the channel, L is the length of the channel, and the Pris Prandtl number is defined as the ratio of the viscous diffusion rate to the thermal diffusion rate as shown [34, 36]:

$$Pr = \frac{\nu}{\alpha} = \frac{\mu * cp}{k} \quad (16)$$

$$D_h = \frac{4\,(\text{cross-sectional area})}{\text{wetted per meter}} \quad (17)$$

2.2.2. Transfer of heat via the membrane layer

Adding the two forms of heat transmission via the membrane, conductive and evaporative, provides the overall heat transfer rate through the membrane [1, 46, 47].

$$Q_m = Q_C + Q_v \quad (18)$$

The overall heat flow through the membrane (Q_m). The heat transfer through the membrane that is conducted (QC). The mass flux via the membrane pores that evaporates (Qv).

The effective thermal conductivity of the membrane, denoted as k_m, is the sum of the gas thermal conductivity (k_g) and the membrane's solid thermal conductivity (ks). It may be determined using the following formula [48]:

$$Q_C = \frac{k_m}{\delta}\,(T_{mf} - T_{mp}) \quad (19)$$

$$k_m = \left(\frac{\varepsilon}{k_g} + \frac{1-\varepsilon}{k_s}\right)^{-1} \quad (20)$$

$$Q_v = J_W * \Delta H_v \quad (21)$$

J_w is permeate flux, ΔH_v is the water vaporization enthalpy, which can be calculated using the [22]:

$$\Delta H_v = 1.7535\,T_{mf} + 2024.3 \quad (22)$$

The overall rate of heat transfers through the membrane (Q_m).

$$Q_m = \frac{k_m}{\delta}\,(T_{mf} - T_{mp}) + J_W * \Delta H_v \quad (23)$$

2.2.3. The movement of heat from the surface of the membrane to the permeate stream

Transfer of convective heat from the surface of the membrane to the permeate stream in the boundary layer region [47, 49, 50].

$$Q_p = h_p * (T_{mp} - T_{bp}) \quad (24)$$

T_{mp} is the surface temperature of the membrane on the permeate side, T_{bp} is the average bulk temperature of the cold permeate stream entering and leaving the system, and h_p is the boundary layer heat transfer coefficient on the permeate side, which is measured in the same way as on the feed side.

While in a steady state, the unknowns in the MD process, such as the feed membrane interface temperature (T_{mf}) and the permeate membrane interface temperature (T_{mp}), can be calculated in Eqs. 25 and 26 and Using the assumed temperature and the steps shown in Fig. 2, the following is the steady-state formula for the overall heat transfer via the DCMD method [22, 33, 51]:

$$Q_f = Q_m = Q_p \quad (25)$$

The feed and permeate surface temperatures of the membrane are determined by [51-53].

$$T_{mf} = \frac{k_m\left(T_{bp} + \frac{h_f}{h_p}T_{bf}\right) + \delta\,(h_f\,T_{bf} - J_w * \Delta H_V)}{(k_m) + h_f\,(\delta + \frac{k_m}{h_p})} \quad (26)$$

$$T_{mp} = \frac{k_m\left(T_{bf} + \frac{h_p}{h_f}T_{bp}\right) + \delta\,(h_p\,T_{bp} + J_w * \Delta H_V)}{(k_m) + h_p\,(\delta + \frac{k_m}{h_f})} \quad (27)$$

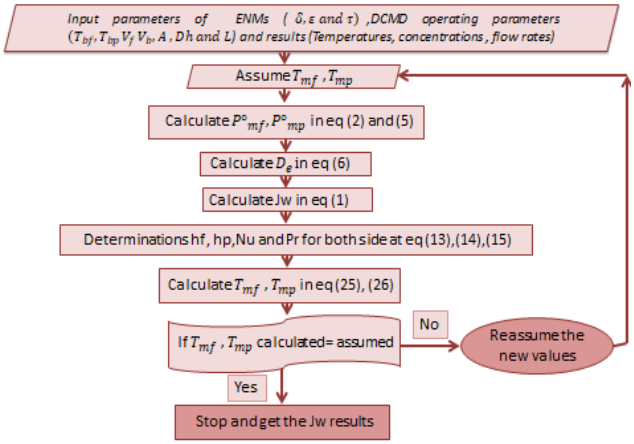

Fig. 2. The following algorithm's flow diagram for predicting the DCMD permeate flux (Jw)

3- Experimental methods (DCMD performance)

Fig. 3 shows the graphical layout of the experimental setup of the direct contact membrane distillation (DCMD) method. Fig. 5 shows a picture of the DCMD process. The run of the DCMD experiment was curried for about 5 h. A peristaltic pump was used in the DCMD process to deliver the hot feed solution to the top side of the flat sheet-produced membrane at a flow rate controlled by a control valve with a pressure gauge on the right side. At the same time, the vapor water was passing through the membrane because of the driving force of partial pressure at the sides of the membrane to with cold distillate, the cold distillate water with the vapor water circle in the bottom side from module also by a peristaltic pump through a control valve that regulates the flow rate with

and pressure gauge in the left side. The chiller and bath are carried handmade.

Using a water bath, the prepared saltwater in a 500 ml glass tank was heated to various degrees (i.e. 35-55 °C), and a chiller was set at a constant 10 °C. The Flat sheet membrane module of DCMD was designed and constructed in Italy in an area of about (6*6) cm^2, as shown in Fig. 4.

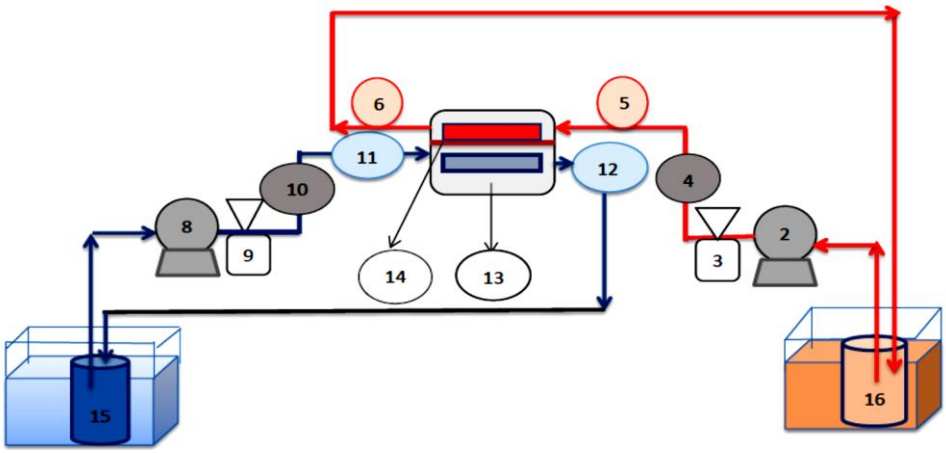

1.	Bath for feed	2.	Pump for feed
3.	Rotameter for feed	4.	Inlet pressure gauge for feed
5.	Inlet temperature sensor for feed	6	Outlet temperature sensor for feed
7.	Chiller for permeate mm	8.	Pump for chiller (permeate)
9.	Rotameter for chiller (permeate)	10.	Inlet pressure gauge for permeate
11.	Inlet temperature sensor for permeate	12.	Outlet temperature sensor for permeate
13.	Membrane module	14.	Membrane
15.	Tank for permeate	16.	Tank for feed

Fig. 3. Experimental setup for the DCMD procedure

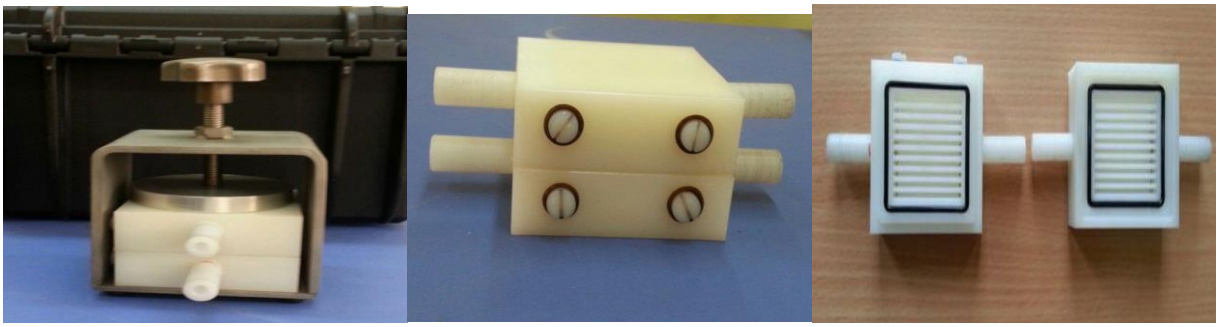

Fig. 4. Pictures of the membrane module from the outside and inside

Fig. 5. Picture of the DCMD process

3.1. The characteristics of nanofiber membrane

The characteristics of the prepared nanofiber membrane by electrospinning double layer. The first (base) layer was hydrophobic polyvinylidene fluoride (PVDF) based electrospun nanofibers and the second (top) layer was hydrophobic polymethyl methacrylate (PMMA) based electrospun nanofibers at 30% PMMA and 10% PAN by (25PAN:75PMMA) [54] and adding silica nanoparticles at 3.5% in PMMA, data presented in Table 1.

3.1.1. AFM

The surfaces of the manufactured nonwoven nanofiber membranes as analyzed by AFM for roughness, an important factor in determining the membrane's wettability and fouling resistance [55] as shown in Fig. 6. The membrane's surface roughness on average (Ra) found about 539.5 nm and the size of the pore at 323.4 µm.

3.1.2. Contact angle (CA)

A membrane's hydrophobicity can be measured by gauging the water's contact angle with the surface [56, 57] and images obtained using, the contact angle in Fig. 7 about 152º.

3.1.3. Scanning Electron Microscope (SEM)

An important factor for the surface characteristics of the manufactured nonwoven nanofiber membranes [54] as shown in Fig. 8 that the measured fiber size average is about 150.4 nm.

The permeate flux is evaluated in the following equation.

$$J_v = (V * \rho)/(A * t) \quad (28)$$

The membrane's effective surface area (m^2) (A), the volume of collected water (l) (V), the water density (kg/m^3) (ρ), the time it takes for water to be collected (hr) (t), and the water vapor permeation flux (Jv) are all variables in this equation. An electrical conductivity meter (a German-made Model DDS 307) was used to monitor the salt concentrations of the feed and permeate going into and out of the membrane module. The salt rejection was determined using the following formula [54, 58].

$$R(\%) = [1 - (C_P/C_F)] \quad (29)$$

Here, R refers to salt rejection, C_P to permeate solution concentration, and C_F for the concentration solution of feed [54, 58].

Table 1. Characteristics of the prepared membrane by electrospinning

Membrane type	(25PAN:75PMMA) with 3.5% silica in PMMA
Average pore size	323.4(µm)
Thickness	100 (µm)
Porosity	82(%)
Contact angle	152◦
Roughness	539.5 (nm)
Membrane area A	36(cm^2)

The DCMD performance was examined in this work with feed temperatures ranging from 35 to 55°C at several temperatures (35,40,45,50 and 55°C), using the flow rate of feed of 0.2, 0.3, 0.4 and 0.6 L/min with feed salt concentrations at 70, 140 and 210 g/L) to doing the main tests on desalination of salt water [54]. These parameters were selected based on previous studies some of which are listed in Table 2.

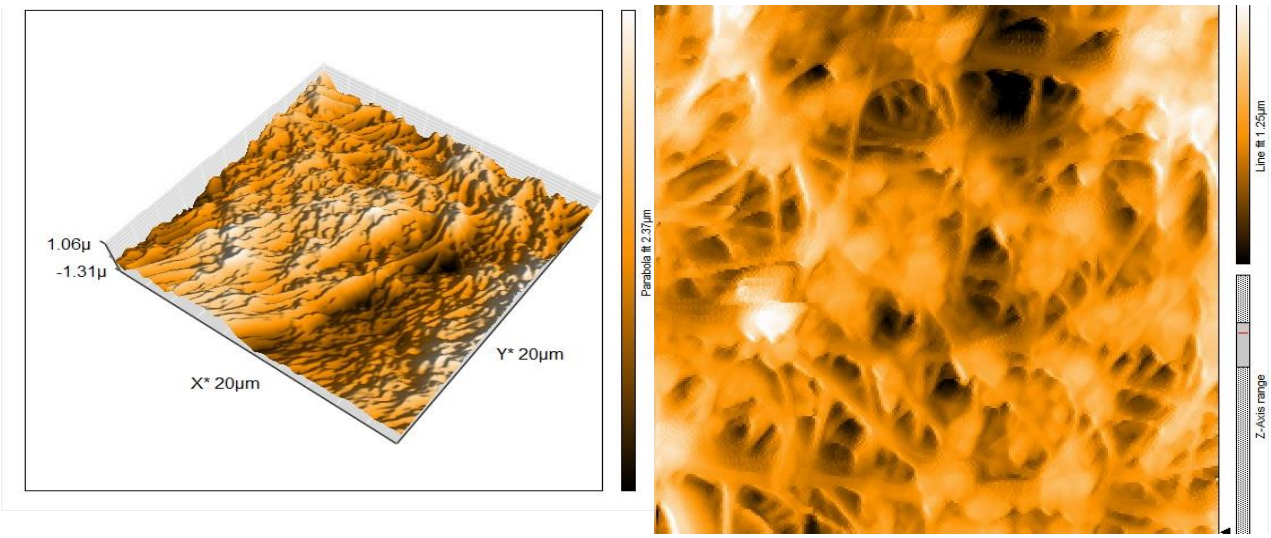

Fig. 6. AFM image of the prepared double-layers (25PVDF: 75PMMA) with 3.5 % silica in PMMA nonwoven nanofibers membranes and analyzing surface roughness

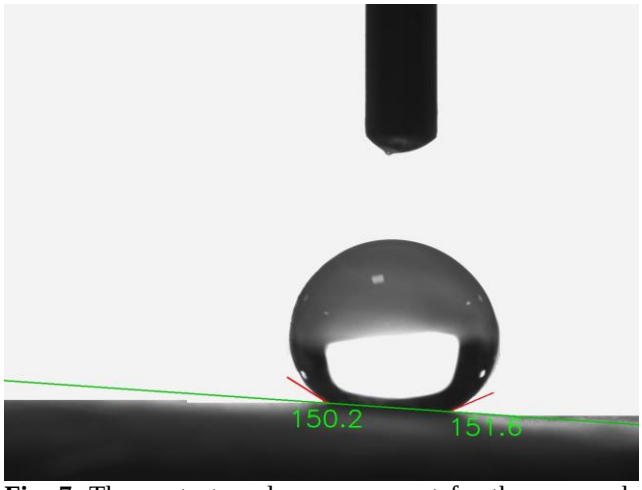

Fig. 7. The contact angle measurement for the prepared double-layers (25PVDF: 75PMMA) with 3.5 % silica in PMMA nonwoven nanofibers membranes (Super Hydrophobic)

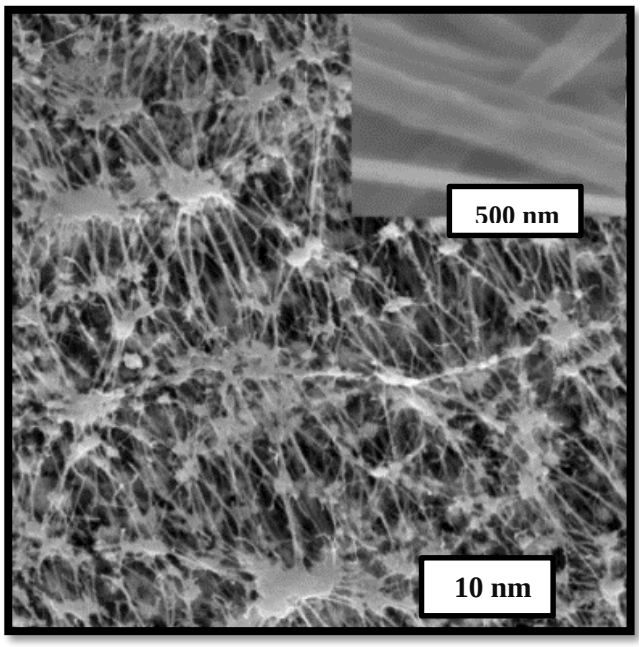

Fig. 8. The SEM of the prepared double-layers (25PVDF: 75PMMA) with 3.5 % silica in PMMA nonwoven nanofibers membranes

4- Results and discussion

The efficiency of the DCMD process is highly dependent on the operating conditions. A set of tests was conducted to evaluate DCMD's performance by studying the effect of operational parameters on the permeate flux. In this study, three variables were considered at varying levels: feed temperature (35–55◦C), feed flow rate (0.2–0.6 L/min), and feed concentration (0–210 g/L).

4.1. Effect of feed temperature

As seen in Fig. 9, the permeate flux varies with feed temperature for various concentrations. As the feed solution concentration changed from 0 to 70, 140 to 210 g/L, the feed temperature varied from 35 to 55, but the feed flow rate was kept constant at 0.6 L/min. Fig. 9 shows that the permeate flux grows as feed temperature increases for all salt concentrations. There is a significant connection between the feed temperature and the evaporation rate. Fig. 9 indicates that the permeate flux grew exponentially with temperature. This is because the driving force is greater at higher temperatures, which causes the partial pressure of the vapor to increase exponentially with temperature. The relationship between feed temperature and vapor pressure, predicted by Antoine's equation, which shows an exponential relationship, may account for this behavior.

For a solution of 70 g/L NaCl, Fig. 10 shows how the feed temperature affects the permeate conductivity and salt rejection. As the feed temperature increased, the pore size expanded slightly, leading to a slight rise in the permeate conductivity. The investigated temperature rise range had little effect on the membrane's pore size and wetting process, although 99.99% salt rejection was still obtained that agreed with [22, 59].

4.2. Effect of feed flow rate

The effect of feed flow rate on membrane performance as a function of different feed concentrations at 65°C feed temperature is shown in Fig. 11 and Fig. 12. Fig. 12 demonstrates that raising the feed flow rate led to increased permeate flux, consistent with earlier research [59, 60].

Because of the increased Reynolds number, which decreased the temperature and concentration boundary layer thickness and consequently led to lower heat and mass transfer resistances, the permeate flux increased with the flow rate. The electric conductivity increased with increasing feed flow rate across all feed temperatures, but salt rejection was marginally reduced (Fig. 12). This is because the pressure changes as a function of the flow rate, which could explain how a little wetting could happen when the pressure changes are substantial that agreed with literature [59].

4.3. Effect of feed concentration

As seen in Fig. 13, the penetration flux decreases as the salt concentration increases. Because a concentration boundary layer, which runs parallel to the thermal boundary layer, formed due to the NaCl particles. To limit the permeate flux, the concentration and temperature boundary layers work together as a barrier to vapor transfer, reducing the driving force for evaporation. As predicted, the DCMD flow decreases as salt concentration rises. The decrease in vapor pressure in the feed is the cause of this [22, 61].

Fig. 14 shows that as the NaCl concentration was raised, the permeate conductivity rose rapidly while the salt rejection decreased. Low entry pressure (LEP) conditions (water will pass through the membrane if there is a pressure more significant than the membrane's entry

pressure) led to an increase in penetration conductivity under more significant concentrations. As the feed concentration increased, the permeation conductivity also rose and 99.97% in terms of salt rejection. The electric conductivity increased with increasing feed flow rate across all feed temperatures, but the salt rejection was marginally reduced **(**Fig. 12**).** This is because the pressure changes as a function of the flow rate, which could explain how a little wetting could happen when the pressure changes are substantial that agreed with the literature [18, 22, 59, 62].

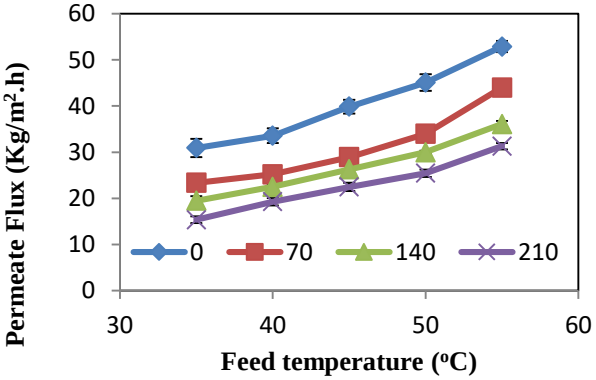

Fig. 9. Feed temperature's influence on permeate flux at varying feed concentrations, with a flow rate of 0.6 L/min

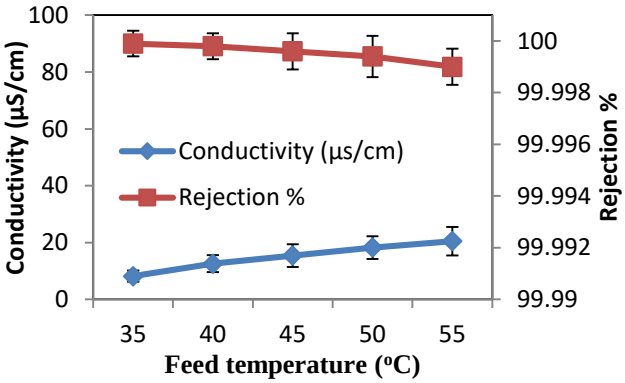

Fig. 10. Conductivity and salt rejection as a function of feed temperature for a 70 g/L and 0.6 L/min feed solution

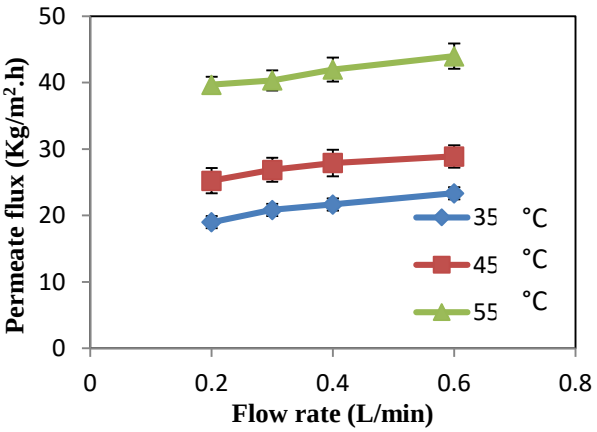

Fig. 11. Permeate flux as a function of feed flow rate at a range of feed temperatures and a concentration of 70 g/L

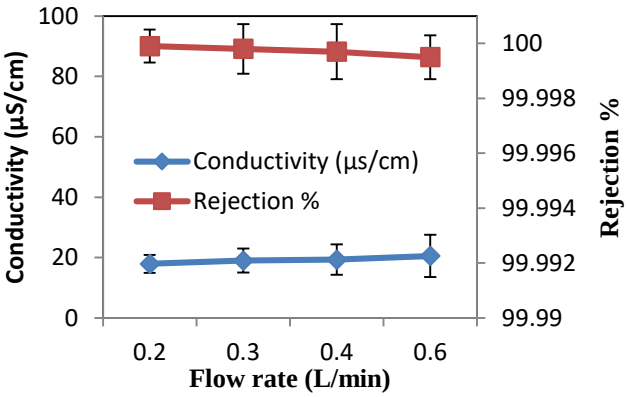

Fig. 12. Conductivity and rejection as a function of feed flow rate for a manufactured membrane at a feed concentration of 70 g/L and a feed temperature of 55 °C

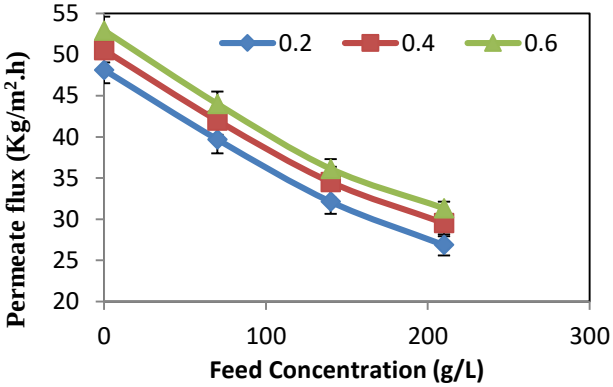

Fig. 13. Changes in permeate flux as a function of feed concentration at various feed flow rates and feed temperatures (55 °C)

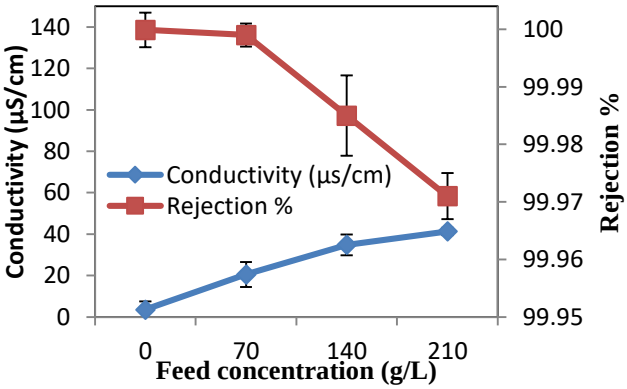

Fig. 14. Conductivity and salt rejection as a function of feed concentration in a feed solution at 55 °C feed temperature and 0.6 L/min feed flow rate

4.4. Statistical method

In order to account for the additional mass transfer resistance that might not be immediately apparent during the MD operation, a MATLAB-based model of simultaneous heat and mass transfer was created for a DCMD system. This model takes into account the operating conditions (such as temperature and concentration) and represents them through a hypothetical

path φ across the membrane (φ= δ ∗ τ), where δ is the thickness of the membrane and τ is the tortuosity. As a matter of fact, this parameter would be utilized to convey the operational variation of membrane features. In order to compare the DCMD process's performance with the model that was established, an experimental investigation was carried out. This investigation utilized a high salty water supply with a NaCl concentration of up to 210 g/L under different operation circumstances.

4.5. Theoretical results

The proposed mathematical model was validated by comparing its simulated results with the experimental data. At a produced membrane porosity of 82%, Fig. 15 shows the experimental data compared to the predicted model for 0,70, 140, and 210 g/L NaCl solutions. This figure shows a slight difference between the experimental and theoretical results on both feed concentrations. Fig. 16 shows the results of comparing the model's predictions with experimental data on the permeate flux.

The reason for the difference that is very slight between the theoretical and the experimental is that the fibers inside the membrane will suffer from a phenomenon called swelling, i.e. the fibers swelling that slightly expended in hot water, causing a decrease in the pore size, which causes a decrease in the amount of output, as well as a loss of the very little heat, which also leads to a decrease in the flow then decrease in permeate flux that agreed with[63, 64].

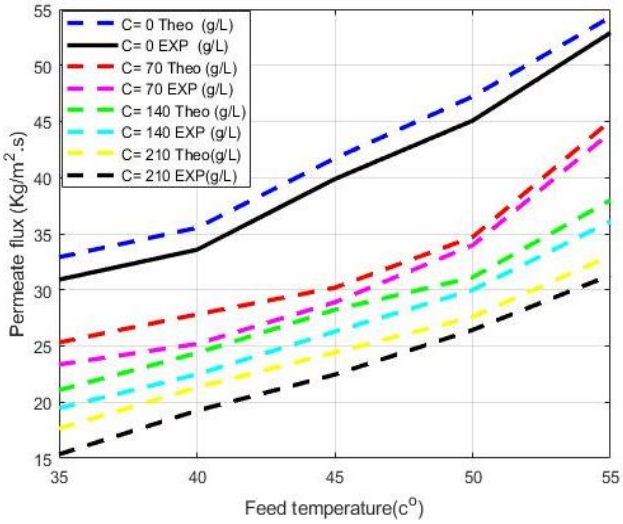

Fig. 15. Permeation flux as a function of feed temperature at concentrations of 0,70.140 and 210 g/L NaCl and feed rates of 0.6 L/min

4.6. Thermal efficiency (Ƞ)

A theoretical model was proposed for evaluating the DCMD process's thermal efficiency. Fig. 17 shows that the feed temperature significantly affected the thermal efficiency; hence, raising the feed temperature increased the process's thermal efficiency. The reason is that when the temperature rises, the heat lost by conduction is reduced compared to the heat lost through vaporization, which is a function of thermal efficiency. Eq. 35 shows that heat conduction, on the other hand, is inversely related to thermal efficiency (Eq. 29) [22].

$$\eta = \frac{(J_w * \Delta H_v)}{(\frac{k_m}{\delta}(T_{mf} - T_{mp}) + (J_w * \Delta H_v)} \quad (30)$$

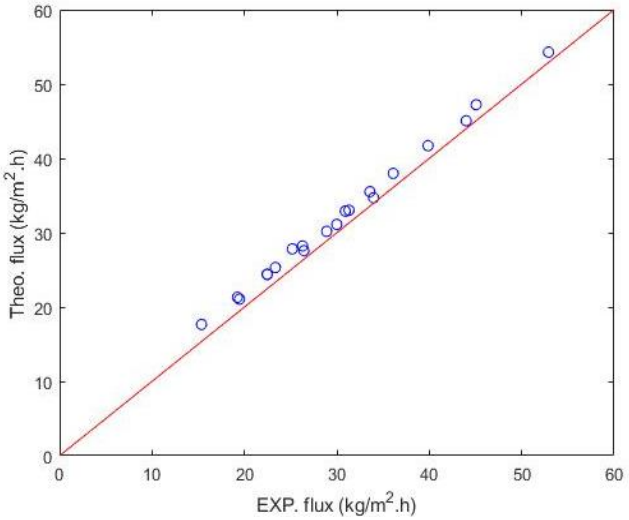

Fig. 16. A Comparison of the permeate flux experimental data the model's predicted values

4.7. Gain output ratio (GOR)

Another important factor in MD, especially when heat recovery is involved, is the gain output ratio (GOR). GOR is a measure that shows how efficiently the following equation can be used to evaluate the thermal energy [65, 66]:

$$GOR = \frac{(J_w * \Delta H_v) * A}{Q_{in}} \quad (31)$$

The following equation determines the effective area of the membrane (A) and the total heat used by the system

$$Q_{\text{in}} = m_{\text{f}} * C_{\text{p}} (T_{\text{pf in}} - T_{\text{pf out}}) \quad (32)$$

Where m_f represents the feed solution's mass flow rate and C_p its specific heat capacity, $T_{bf\ in}$ and $T_{bf\ out}$ represent the hot feed temperatures entering and leaving the system, respectively. As shown in Fig. 16, the gain output ratio is proportional to the feed temperature. When the feed temperature was raised, the GOR value also rose. According to the, a direct relationship appeared between the mass flux and the GOR value, which was caused by a rise in the partial pressure difference.

4.8. Temperature polarization coefficient (TPC)

The TPC ranged from 0 to 1, with higher values indicating lower affected by temperature polarization. In Fig. 17, we can see that the feed temperature has an inverse relationship with in addition to the TPC's value. The TPC value becomes higher when the feed temperature changes significantly. The temperature or

thermal polarization coefficient (TPC) is utilized when describing a process's thermal efficiency [66]. Table 2 and Fig. 17 allowed me to compare to prior research and find a very close match with [22].

$$TPC = \frac{T_{mf}-T_{mp}}{T_{bf}-T_{bp}} \quad (33)$$

The performance of the membranes predicted by this study is compared to the performance of the selected membrane values from the literature in Table 2. In addition to the most crucial operating characteristics, Table 2 also includes feed concentration, feed temperature, and feed flow rate. It is clear that the permeation flow predicted by the given model for the membranes is realistic and agrees well with the majority of membranes' permeation fluxes reported in the literature.

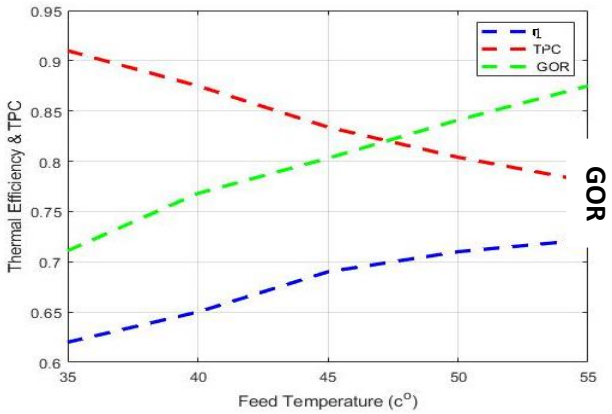

Fig. 17. Thermal efficiency (η) at different feed temperatures, 70 g/L NaCl, and 0.6 L/min, as well as the DCMD system's gain output ratio (GOR) and thermal polarization coefficient (TPC)

Table 2. Various membranes from the literature are compared to the projected model's performance in this study

Membrane Name *	Temp. of Feed (°C)	Conc. of Feed (g/L)	Flow Rate of Feed (L/min)	Exp. Flux (kg/m².h)	Ref.
PVDF-*co*-HFP	47–67	0–100	0.35–0.55	16.35	[62]
DHPVC-g-PEA	65	200	0.6	32	[59]
PVDF-co-HFP	45–65	0–100	0.2 – 0.6	17.3	[18]
PTFE	45–65	0–200	0.3 – 1.07	5.1-17.3	[22]
PVDF	50	35	0.6	21	[38]
M4-2(PDMS)	70	35	1	43	[66]
PTFE	40–90	4.65	0.14–100	55–72	[67]
PVDF	80	0.45	6	51.5	[68]
PTFE	130	10	0.5	195	[69]
PTFE-CNTs	70	34	-	69	[70]
PP	40-60	-	0.5–1.7	5–25	[71]
PVDF-HFP/SiNPs	80	35	1.166	48.6	[72]
PP	85–90	10–100	25	60–79	[73]
PTFE	60	Seawater	4.5	45.5	[74]
PTFE + TiO2NF	50–80	0–100	-	7–12.2	[75]
PTFE	38	Various	11–22	2–5	[76]
PTFE	70	35	Re = 500–1500	47.8–86.8	[77]
PTFE-PP	60	30	0.04	12.2	[78]
PVDF PTFE+PET+CS	60	20	0.5	19	[79]
PMMA ,PVDF SiO_2	35–55	0–210	0.2–0.6	16- 53	Present work

* PVDF-*co*-HFP: Poly vinylidene fluoride-co-hexafluoropropylene; DHPVC-g-PEA: Polyvinyl chloride-graft-poly ethyl acrylate; PVDF: polyvinylidene difluoride; PDMS: polydimethylsiloxane; CNTs: carbon Nanotubes; PP: polypropylene; PVDF-HFP/SiNPs: poly(vinylidene fluoride-co-hexafluropropylene)/Silica nanoparticles; F-TNF: Fluorinated Titania; PET: polyethylene support layer; CS-PEO: chitosan-polyethylene oxide.

5- Conclusions

A DCMD flat sheet electrospun nanofiber membrane was simulated and experimentally studied. The built DCMD process model considered the module dimensions, operating conditions, and membrane characteristics. This model used theoretical and experimental approaches to investigate how feed temperature, flow rate, and concentration affected permeate flux. The permeation flux over the membrane was positively affected when changing the feed temperature and flow rate. However, the feed concentration was negative. When the feed temperature went up from (35-55) ºC, the DCMD thermal efficiency increased from (0.62-0.73) and the DCMD system's temperature polarization coefficient went down sharply from (0.91 to 0.78) at 0.6 L/min feed flow rate, fed a concentration of 70 g/L and the constructed membrane achieved a high salt rejection of around 99.99% and 43 kg/m².h. While at the highest salt concentration of feed at 210 g/L, the constructed recorded salt rejection of about 99.97 and 32 kg/m².h due to increases in the concertation polarization on the surface of the membrane that is less from passing the vapor through the pore size then causes little shortage in permeate flux.

Reference

[1] A. Khalifa, H. Ahmad, M. Antar, T. Laoui, and M. Khayet, "Experimental and theoretical investigations on water desalination using direct contact membrane distillation," *Desalination*, vol. 404, pp. 22-34, 2017/02/17/ 2017, https://doi.org/10.1016/j.desal.2016.10.009

[2] M. Al-Furaiji, U. Karim, D. Augustijn, B. Waisi, and S. Hulscher, "Evaluation of water demand and supply in the south of Iraq," *Journal of Water Reuse and Desalination*, vol. 6, pp. 214-226, 03/01 2016, https://doi.org/10.2166/wrd.2015.043

[3] R. Mahadeva *et al.*, "Water desalination using PSO-ANN techniques: A critical review," *Digital Chemical Engineering*, vol. 9, p. 100128, 2023/12/01/ 2023, https://doi.org/10.1016/j.dche.2023.100128

[4] A. Mittal, R. Brajpuriya, and R. Gupta, "Solar steam generation using hybrid nanomaterials to address global environmental pollution and water shortage crisis," *Materials Today Sustainability*, vol. 21, p. 100319, 2023/03/01/ 2023, https://doi.org/10.1016/j.mtsust.2023.100319

[5] S. Al-Amshawee, M. Y. B. M. Yunus, A. A. M. Azoddein, D. G. Hassell, I. H. Dakhil, and H. A. Hasan, "Electrodialysis desalination for water and wastewater: A review," *Chemical Engineering Journal*, vol. 380, p. 122231, 2020/01/15/ 2020, https://doi.org/10.1016/j.cej.2019.122231

[6] G. Amy *et al.*, "Membrane-based seawater desalination: Present and future prospects," *Desalination*, vol. 401, pp. 16-21, 2017/01/02/ 2017, https://doi.org/10.1016/j.desal.2016.10.002

[7] M. Nair and D. Kumar, "Water desalination and challenges: The Middle East perspective: a review," *Desalination and Water Treatment*, vol. 51, no. 10-12, pp. 2030-2040, 2013/02/01 2013, https://doi.org/10.1080/19443994.2013.734483

[8] M. Shatat, M. Worall, and S. Riffat, "Opportunities for solar water desalination worldwide: Review," *Sustainable Cities and Society*, vol. 9, pp. 67-80, 2013/12/01/ 2013, https://doi.org/10.1016/j.scs.2013.03.004

[9] S. Fadhil *et al.*, "Seawater desalination using PVDF-HFP membrane in DCMD process: assessment of operating condition by response surface method," *Chemical Engineering Communications*, vol. 206, no. 2, pp. 237-246, 2019/02/01 2019, https://doi.org/10.1080/00986445.2018.1483349

[10] M. K. Shahid *et al.*, "A Review of Membrane-Based Desalination Systems Powered by Renewable Energy Sources," *Water*, vol. 15, no. 3, p. 534, 2023. https://doi.org/10.3390/w15030534

[11] S. Yarlagadda, V. G. Gude, L. M. Camacho, S. Pinappu, and S. Deng, "Potable water recovery from As, U, and F contaminated ground waters by direct contact membrane distillation process," *Journal of Hazardous Materials*, vol. 192, no. 3, pp. 1388-1394, 2011/09/15/ 2011, https://doi.org/10.1016/j.jhazmat.2011.06.056

[12] C. Yang *et al.*, "Effective evaporation of CF4 plasma modified PVDF membranes in direct contact membrane distillation," *Journal of Membrane Science*, vol. 482, pp. 25-32, 2015/05/15/ 2015, https://doi.org/10.1016/j.memsci.2015.01.059

[13] D. Cheng, W. Gong, and N. Li, "Response surface modeling and optimization of direct contact membrane distillation for water desalination," *Desalination*, vol. 394, pp. 108-122, 2016/09/15/ 2016, https://doi.org/10.1016/j.desal.2016.04.029

[14] J. Sanmartino, M. Khayet, and M. C. García-Payo, 'Desalination by Membrane Distillation,' *Emerging Membrane Technology for Sustainable Water Treatment* 2016, pp. 77-109. https://doi.org/10.1016/B978-0-444-63312-5.00004-8

[15] T. Y. Cath, V. D. Adams, and A. E. Childress, "Experimental study of desalination using direct contact membrane distillation: a new approach to flux enhancement," *Journal of Membrane Science*, vol. 228, no. 1, pp. 5-16, 2004/01/01/ 2004, https://doi.org/10.1016/j.memsci.2003.09.006

[16] P. Yadav, R. Farnood, and V. Kumar, "Superhydrophobic modification of electrospun nanofibrous Si@PVDF membranes for desalination application in vacuum membrane distillation," *Chemosphere*, vol. 287, p. 132092, 2022/01/01/ 2022, https://doi.org/10.1016/j.chemosphere.2021.132092

[17] Q. F. Alsalhy, S. S. Ibrahim, and F. A. Hashim, "Experimental and theoretical investigation of air gap membrane distillation process for water desalination," *Chemical Engineering Research and Design*, vol. 130, pp. 95-108, 2018/02/01/ 2018, https://doi.org/10.1016/j.cherd.2017.12.013

[18] N. N. Safi *et al.*, "A Systematic Framework for Optimizing a Sweeping Gas Membrane Distillation (SGMD)," *Membranes*, vol. 10, no. 10, p. 254, 2020. https://doi.org/10.3390/membranes10100254

[19] A. Kayvani Fard, T. Rhadfi, M. Khraisheh, M. A. Atieh, M. Khraisheh, and N. Hilal, "Reducing flux decline and fouling of direct contact membrane distillation by utilizing thermal brine from MSF desalination plant," *Desalination*, vol. 379, pp. 172-181, 2016/02/01/ 2016, https://doi.org/10.1016/j.desal.2015.11.004

[20] A. Alkhudhiri, N. Darwish, and N. Hilal, "Membrane distillation: A comprehensive review," *Desalination*, vol. 287, pp. 2-18, 2012/02/15/ 2012, https://doi.org/10.1016/j.desal.2011.08.027

[21] M. Darman, N. Niknafs, and A. Jalali, "Effect of wavy corrugations on the performance enhancement of direct contact membrane distillation modules: A numerical study," *Chemical Engineering and Processing - Process Intensification*, vol. 190, p. 109421, 2023/08/01/ 2023, https://doi.org/10.1016/j.cep.2023.109421

[22] N. A. M. Ameen, S. S. Ibrahim, Q. F. Alsalhy, and A. Figoli, "Highly Saline Water Desalination Using Direct Contact Membrane Distillation (DCMD): Experimental and Simulation Study," *Water*, vol. 12, no. 6, 2020, https://doi.org/10.3390/w12061575

[23] F. Abu Al-Rub, F. Banat, and K. Bani-Melhem, "Parametric sensitivity analysis of direct contact membrane distillation," *Separation Science and Technology - SEPAR SCI TECHNOL*, vol. 37, pp. 3245-3271, 01/11 2002, https://doi.org/10.1081/SS-120006160

[24] H. Hayer, O. Bakhtiari, and T. Mohammadi, "Simulation of momentum, heat and mass transfer in direct contact membrane distillation: A computational fluid dynamics approach," *Journal of Industrial & Engineering Chemistry*, vol. 21, 06/17 2015, https://doi.org/10.1016/j.jiec.2014.06.009

[25] Y. Zhou, L. Chen, M. Huang, W. Hu, G. Chen, and B. Wu, "Experimental Investigation of the Desalination Process for Direct Contact Membrane Distillation Using Plate and Frame Membrane Module," *Applied Sciences*, vol. 13, no. 16, p. 9439, 2023. https://doi.org/10.3390/app13169439

[26] Z. Kuang, R. Long, Z. Liu, and W. Liu, "Analysis of temperature and concentration polarizations for performance improvement in direct contact membrane distillation," *International Journal of Heat and Mass Transfer*, vol. 145, p. 118724, 2019/12/01/ 2019, https://doi.org/10.1016/j.ijheatmasstransfer.2019.118724

[27] P. Moghaddam Kamrani, O. Bakhtiari, P. Kazemi, and T. Mohammadi, "Theoretical modeling of direct contact membrane distillation (DCMD): effects of operation parameters on flux," *Desalination and Water Treatment*, vol. 56, no. 8, pp. 2013-2022, 2015/11/20 2015, https://doi.org/10.1080/19443994.2014.960461

[28] M. Khayet and C. Cojocaru, "Artificial neural network model for desalination by sweeping gas membrane distillation," *Desalination*, vol. 308, pp. 102–110, 01/02 2013, https://doi.org/10.1016/j.desal.2012.06.023

[29] M. Essalhi and M. Khayet, "Self-sustained webs of polyvinylidene fluoride electrospun nanofibers at different electrospinning times: 2. Theoretical analysis," *Journal of Membrane Science*, vol. 433, pp. 180–191, 04/01 2013, https://doi.org/10.1016/j.memsci.2013.01.024

[30] J. Zhang, N. Dow, M. Duke, E. Ostarcevic, J.-D. Li, and S. Gray, "Identification of material and physical features of membrane distillation membranes for high performance desalination," *Journal of Membrane Science*, vol. 349, pp. 295-303, 03/01 2010, https://doi.org/10.1016/j.memsci.2009.11.056

[31] S. Ibrahim and Q. Alsalhy, "Modeling and Simulation for Direct Contact Membrane Distillation in Hollow Fiber Modules," *AIChE Journal*, vol. 59, 02/01 2013, https://doi.org/10.1002/aic.13845

[32] M. Khayet, "Membranes and theoretical modeling of membrane distillation: A review," *Advances in Colloid and Interface Science*, vol. 164, no. 1, pp. 56-88, 2011/05/11/ 2011, https://doi.org/10.1016/j.cis.2010.09.005

[33] M. Essalhi and M. Khayet, "Self-sustained webs of polyvinylidene fluoride electrospun nanofibers at different electrospinning times: 2. Theoretical analysis, polarization effects and thermal efficiency," *Journal of Membrane Science*, vol. 433, pp. 180-191, 2013/04/15/ 2013, https://doi.org/10.1016/j.memsci.2013.01.024

[34] Z. W. Song and L. Y. Jiang, "Optimization of morphology and perf ormance of PVDF hollow fiber for direct contact membrane distillation using experimental design," *Chemical Engineering Science*, vol. 101, pp. 130-143, 2013/09/20/ 2013, https://doi.org/10.1016/j.ces.2013.06.006

[35] T.-C. Chen, C.-D. Ho, and H.-M. Yeh, "Theoretical modeling and experimental analysis of direct contact membrane distillation," *Journal of Membrane Science*, vol. 330, no. 1, pp. 279-287, 2009/03/20/ 2009, https://doi.org/10.1016/j.memsci.2008.12.063

[36] J. A. Sanmartino, M. Khayet, and M. C. García-Payo, "Chapter 4 - Desalination by Membrane Distillation," in *Emerging Membrane Technology for Sustainable Water Treatment*, N. P. Hankins and R. Singh Eds. Boston: Elsevier, 2016, pp. 77-109. https://doi.org/10.1016/B978-0-444-63312-5.00004-8

[37] M. Khayet, 'Membranes and theoretical modeling of membrane distillation: a review,' *Advances in Colloid and Interface Science*, vol. 164, no. 1-2, pp. 56-88, May 11 2011, https://doi.org/10.1016/j.cis.2010.09.005

[38] J. Phattaranawik, R. Jiraratananon, and A. G. Fane, "Effect of pore size distribution and air flux on mass transport in direct contact membrane distillation," *Journal of Membrane Science*, vol. 215, no. 1, pp. 75-85, 2003/04/15/ 2003, https://doi.org/10.1016/S0376-7388(02)00603-8

[39] Ó. Andrjesdóttir *et al.*, "An experimentally optimized model for heat and mass transfer in direct contact membrane distillation," *International Journal of Heat and Mass Transfer*, vol. 66, pp. 855-867, 2013/11/01/ 2013, https://doi.org/10.1016/j.ijheatmasstransfer.2013.07.051

[40] M. S. El-Bourawi, Z. Ding, R. Ma, and M. Khayet, "A framework for better understanding membrane distillation separation process," *Journal of Membrane Science*, vol. 285, no. 1, pp. 4-29, 2006/11/15/ 2006, https://doi.org/10.1016/j.memsci.2006.08.002

[41] M. Qtaishat, T. Matsuura, B. Kruczek, and M. Khayet, "Heat and mass transfer analysis in direct contact membrane distillation," *Desalination*, vol. 219, no. 1, pp. 272-292, 2008/01/25/ 2008, https://doi.org/10.1016/j.desal.2007.05.019

[42] C.-D. Ho, C.-H. Huang, F.-C. Tsai, and W.-T. Chen, "Performance improvement on distillate flux of countercurrent-flow direct contact membrane distillation systems," *Desalination*, vol. 338, pp. 26-32, 2014/04/01/ 2014, https://doi.org/10.1016/j.desal.2014.01.023

[43] Y. Yun, R. Ma, W. Zhang, A. G. Fane, and J. Li, "Direct contact membrane distillation mechanism for high concentration NaCl solutions," *Desalination*, vol. 188, no. 1, pp. 251-262, 2006/02/05/ 2006, https://doi.org/10.1016/j.desal.2005.04.123

[44] L. Martínez-Díez and M. I. Vázquez-González, "Temperature and concentration polarization in membrane distillation of aqueous salt solutions," *Journal of Membrane Science*, vol. 156, no. 2, pp. 265-273, 1999/04/30/ 1999, https://doi.org/10.1016/S0376-7388(98)00349-4

[45] S. Srisurichan, R. Jiraratananon, and A. G. Fane, "Mass transfer mechanisms and transport resistances in direct contact membrane distillation process," *Journal of Membrane Science*, vol. 277, no. 1, pp. 186-194, 2006/06/01/ 2006, https://doi.org/10.1016/j.memsci.2005.10.028

[46] J. Phattaranawik, R. Jiraratananon, and A. G. Fane, "Heat transport and membrane distillation coefficients in direct contact membrane distillation," *Journal of Membrane Science*, vol. 212, no. 1, pp. 177-193, 2003/02/15/ 2003, https://doi.org/10.1016/S0376-7388(02)00498-2

[47] L. Francis, N. Ghaffour, A. A. Alsaadi, and G. L. Amy, "Material gap membrane distillation: A new design for water vapor flux enhancement," *Journal of Membrane Science*, vol. 448, pp. 240-247, 2013/12/15/ 2013, https://doi.org/10.1016/j.memsci.2013.08.013

[48] I. Janajreh, D. Suwwan, and R. Hashaikeh, "Assessment of direct contact membrane distillation under different configurations, velocities and membrane properties," *Applied Energy*, vol. 185, pp. 2058-2073, 2017/01/01/ 2017, https://doi.org/10.1016/j.apenergy.2016.05.020

[49] J. Swaminathan, H. W. Chung, D. Warsinger, and J. V, "Membrane distillation model based on heat exchanger theory and configuration comparison," *Applied Energy*, vol. 184, pp. 491-505, 12/01 2016, https://doi.org/10.1016/j.apenergy.2016.09.090

[50] A. Alhathal Alanezi, A. Sharif, M. Sanduk, and A. Khan, "Experimental Investigation of Heat and Mass Transfer in Tubular Membrane Distillation Module for Desalination," *International Scholarly Research Network Chemical Engineering*, vol. 2012, p. 8, 03/21 2012, https://doi.org/10.5402/2012/738731

[51] W. Ni, Y. Li, J. Zhao, G. Zhang, X. Du, and Y. Dong, "Simulation Study on Direct Contact Membrane Distillation Modules for High-Concentration NaCl Solution," *Membranes*, vol. 10, no. 8, p. 179, 2020. https://doi.org/10.3390/membranes10080179

[52] M. Khayet and T. Matsuura, "Membrane distillation: principles and applications. 2011," ed: Elsevier. https://doi.org/10.1016/C2009-0-17487-1

[53] E. Ali, J. Orfi, A. Najib, and O. Hamdaoui, "Understanding the dynamic behavior and the effect of feeding policies of a direct contact membrane distillation for water desalination Understanding the dynamic behavior and the effect of feeding policies of a direct contact membrane distillation for water desalination," *Chemical Engineering Communications*, vol. 208, 10/05 2021, https://doi.org/10.1080/00986445.2020.1814754

[54] B. I. W. Nawras N. Safi, "Preparation of electrospun double-layer PVDF:PMMA membrane non-woven nanofibers for desalination by membrane distillation process," *Desalination and Water Treatment*, pp. 1–10, 2023, https://doi.org/10.5004/dwt.2023.30063

[55] Nawras N. Safi 1, , and B. I. Waisi, 'Enhanced Hydrophobic Double-layer Nanofibers Membranes for Direct Contact Membrane Distillation,' *Ecological Engineering & Environmental Technology* 2024, 25(4), 325–335, https://doi.org/10.12912/27197050/184224

[56] R. S. Hebbar, A. M. Isloor, and A. F. Ismail, "Chapter 12 - Contact Angle Measurements," in *Membrane Characterization*, N. Hilal, A. F. Ismail, T. Matsuura, and D. Oatley-Radcliffe Eds.: Elsevier, 2017, pp. 219-255, https://doi.org/10.1016/B978-0-444-63776-5.00012-7

[57] A. Asadinezhad, M. Lehocký, P. Sáha, and M. Mozetič, "Recent Progress in Surface Modification of Polyvinyl Chloride," *Materials*, vol. 5, no. 12, pp. 2937-2959, 2012. https://doi.org/10.3390/ma5122937

[58] D. S. S. I. Dr. Qusay Fadhel Abdul Hameed Alsalhy and M. S. S. R. AlKurwi, 'Saline Water Desalination by Vacuum Membrane Distillation,' *Conference: The 2nd Arab Water Conference and Exhibition 27-29 May 2014*.,At: At The Ritz-Carlton Doha, 2014.

[59] S. S. Hussein, S. S. Ibrahim, M. A. Toma, Q. F. Alsalhy, and E. Drioli, "Novel chemical modification of polyvinyl chloride membrane by free radical graft copolymerization for direct contact membrane distillation (DCMD) application," *Journal of Membrane Science*, vol. 611, p. 118266, 2020/10/01/ 2020, https://doi.org/10.1016/j.memsci.2020.118266

[60] L. Martínez, "Comparison of membrane distillation performance using different feeds," *Desalination*, vol. 168, pp. 359-365, 2004/08/15/ 2004, https://doi.org/10.1016/j.desal.2004.07.022

[61] S. Shukla *et al.*, "Sweep gas membrane distillation in a membrane contactor with metallic hollow-fibers," *Journal of Membrane Science*, vol. 493, pp. 167-178, 11/01 2015, https://doi.org/10.1016/j.memsci.2015.06.040

[62] M. J. Jamed, A. Alhathal Alanezi, and Q. F. Alsalhy, "Effects of embedding functionalized multi-walled carbon nanotubes and alumina on the direct contact poly(vinylidene fluoride-co-hexafluoropropylene) membrane distillation performance," *Chemical Engineering Communications*, vol. 206, no. 8, pp. 1035-1057, 2019/08/03 2019, https://doi.org/10.1080/00986445.2018.1542302

[63] J. Širc *et al.*, "Morphological Characterization of Nanofibers: Methods and Application in Practice," *Journal of Nanomaterials*, vol. 2012, p. 327369, 2012/11/01 2012, https://doi.org/10.1155/2012/327369

[64] J. M. Preston and M. V. Nimkar, "MEASURING THE SWELLING OF FIBRES IN WATER," *Journal of the Textile Institute Proceedings*, vol. 40, no. 7, pp. P674-P688, 1949/07/01 1949, https://doi.org/10.1080/19447014908664692

[65] A. Criscuoli, "Improvement of the Membrane Distillation performance through the integration of different configurations," *Chemical Engineering Research and Design*, vol. 111, pp. 316-322, 2016/07/01/ 2016, https://doi.org/10.1016/j.cherd.2016.05.020

[66] L.-F. Ren, F. Xia, J. Shao, X. Zhang, and J. Li, "Experimental investigation of the effect of electrospinning parameters on properties of superhydrophobic PDMS/PMMA membrane and its application in membrane distillation," *Desalination*, vol. 404, pp. 155-166, 2017/02/17/ 2017, https://doi.org/10.1016/j.desal.2016.11.023

[67] Y.-D. Kim, K. Thu, N. Ghaffour, and K. Choon Ng, "Performance investigation of a solar-assisted direct contact membrane distillation system," *Journal of Membrane Science*, vol. 427, pp. 345-364, 2013/01/15/ 2013, https://doi.org/10.1016/j.memsci.2012.10.008

[68] S. Meng, J. Mansouri, Y. Ye, and V. Chen, "Effect of templating agents on the properties and membrane distillation performance of TiO2-coated PVDF membranes," *Journal of Membrane Science*, vol. 450, pp. 48-59, 2014. https://doi.org/10.1016/j.memsci.2013.08.036

[69] G. P. Thiel, E. W. Tow, L. D. Banchik, H. W. Chung, and J. H. Lienhard, "Energy consumption in desalinating produced water from shale oil and gas extraction," *Desalination*, vol. 366, pp. 94-112, 2015/06/15/ 2015, https://doi.org/10.1016/j.desal.2014.12.038

[70] M. Bhadra, S. Roy, and S. Mitra, "Flux enhancement in direct contact membrane distillation by implementing carbon nanotube immobilized PTFE membrane," *Separation and Purification Technology*, vol. 161, pp. 136-143, 2016. https://doi.org/10.1016/j.seppur.2016.01.046

[71] J. Swaminathan, H. W. Chung, D. M. Warsinger, F. A. AlMarzooqi, H. A. Arafat, and J. H. Lienhard V, "Energy efficiency of permeate gap and novel conductive gap membrane distillation," *Journal of Membrane Science*, vol. 502, pp. 171-178, 2016, https://doi.org/10.1016/j.memsci.2015.12.017

[72] D. Hou, D. Lin, C. Ding, D. Wang, and J. Wang, "Fabrication and characterization of electrospun superhydrophobic PVDF-HFP/SiNPs hybrid membrane for membrane distillation," *Separation and Purification Technology*, vol. 189, pp. 82-89, 2017, https://doi.org/10.1016/j.seppur.2017.07.082

[73] A. Boubakri, A. Hafiane, and S. A. T. Bouguecha, "Direct contact membrane distillation: Capability to desalt raw water," *Arabian Journal of Chemistry*, vol. 10, pp. S3475-S3481, 2017/05/01/ 2017, https://doi.org/10.1016/j.arabjc.2014.02.010

[74] S. Adnan, M. Hoang, H. Wang, and Z. Xie, "Commercial PTFE membranes for membrane distillation application: Effect of microstructure and support material," *Desalination*, vol. 284, pp. 297-308, 2012/01/04/ 2012, https://doi.org/10.1016/j.desal.2011.09.015

[75] Y. Fan, S. Chen, H. Zhao, and Y. Liu, "Distillation membrane constructed by TiO2 nanofiber followed by fluorination for excellent water desalination performance," *Desalination*, vol. 405, pp. 51-58, 2017/03/01/ 2017, https://doi.org/10.1016/j.desal.2016.11.028

[76] J.-G. Lee, W.-S. Kim, J.-S. Choi, N. Ghaffour, and Y.-D. Kim, "Dynamic solar-powered multi-stage direct contact membrane distillation system: Concept design, modeling and simulation," *Desalination*, vol. 435, pp. 278-292, 2018/06/01/ 2018, https://doi.org/10.1016/j.desal.2017.04.008

[77] A. M. Alwatban, A. M. Alshwairekh, U. F. Alqsair, A. A. Alghafis, and A. Oztekin, "Performance improvements by embedded spacer in direct contact membrane distillation – Computational study," *Desalination*, vol. 470, p. 114103, 2019/11/15/ 2019, https://doi.org/10.1016/j.desal.2019.114103

[78] I. N. Floros *et al.*, "Enhancement of Flux Performance in PTFE Membranes for Direct Contact Membrane Distillation," *Polymers*, vol. 12, no. 2, p. 345, 2020. https://doi.org/10.3390/polym12020345

[79] J. Li *et al.*, "Fabrication of triple layer composite membrane and its application in membrane distillation (MD): Effect of hydrophobic-hydrophilic membrane structure on MD performance," *Separation and Purification Technology*, vol. 234, p. 116087, 2020/03/01/ 2020, https://doi.org/10.1016/j.seppur.2019.116087

دراسة نظرية وتجريبية لطريقة التقطير الغشائي المباشر للتحلية باستخدام اغشية نانوية عالية الرفض للماء

نورس نبيل صافي [١، *]، بسمة اسماعيل ويسي [٢]

١ وزارة الاعمار والاسكان والبلديات العامة، العراق
٢ قسم الهندسة الكيمياوية، كلية الهندسة، جامعة بغداد، العراق

الخلاصة

يركز هذا البحث على أداء نظام التقطير الغشائي بالاتصال المباشر (DCMD) تجريبياً ونظرياً. ويستخدم هذا النظام غشاء نانوي نافر فائق عالي الرفض للماء لتحلية المياه. وأُجريت تحقيقات في كيفية تأثر تركيز التغذية ومعدل تدفق التغذية ودرجة حرارة المحلول بتدفق البخار. وحقق تطبيق أسلوب الكيان التشغيلي المعين (تاغوشي) الاستخدام الإحصائي الأمثل لأداء عملية إدارة النظام. وبالإضافة إلى ذلك، وصف نموذج نظري لدراسة النقل الكتلي والحرارة في إطار نظام DCDM. وفي حين أن تركيز العلف (٠-٢١٠ غرام/لتر) أثر تأثيرا كبيرا على التدفق، فإن درجة حرارة العلف (٣٥-٥٥ درجة مئوية) ومعدل التدفق (٠,٢-٠,٦ لتر/دقيقة) هي الغالبة على التأثير على أداء النظام. وقد حل النموذج المنشأ رقميا عملية DCMD باستخدام برنامج MATLAB، ووصفه بأنه نظام من المعادلات غير الخطية. واستُخدمت ظروف تشغيل مختلفة للتحقيق في كفاءة الغشاء النانوني الليفي في معالجة ٢١٠ غرام/لتر من المياه المالحة. وقد أثر تغيير درجة حرارة التغذية والتركيز على المسار المقترح افتراضياً عبر الغشاء، وفقاً لنتائج المحاكاة المعروضة في هذه البحث. ولوحظ وجود اتفاق ممتاز بين نتائج التجربة والنتائج المتوقعة للنموذج المبني. وحافظت كل حالة على معدل رفض مرتفع للملح (أكثر من ٩٩,٩ في المائة). ونتج عن مشروع DCMD نسبة زيادة في الناتج (GOR) قدرها ٠,٨٧ ومعامل استقطاب في درجة الحرارة تتراوح بين ٠,٧٨ و ٠,٩١. وحقق النظام كفاءة حرارية قصوى قدرها ٧٣,٥ في المائة.البارامترات المثلى، وهي ٧٠ غرام/لتر، و٠,٦ لتر/دقيق، و٥٥ درجة مئوية.

الكلمات الدالة: موديل رياضي، اغشية عالية الرفض للماء، التقطير الغشائي.